Equilibrium geometries, electronic structure, and magnetic properties of Ni_nSn clusters $(n=1-12)$

M. D. Deshpande,[1,*] Swapna Roy,[1] and D. G. Kanhere[2]

[1]*Department of Physics, H.P.T. Arts and R.Y.K. Science College, Nasik 422005, Maharashtra, India*
[2]*Department of Physics and Centre for Modeling and Simulation, University of Pune, Pune 411007, Maharashtra, India*
(Received 22 June 2007; published 16 November 2007)

Equilibrium geometries and the electronic properties of Ni_nSn $(n=1-12)$ clusters have been studied by using spin density functional theory with generalized gradient approximation. The results show that a single tin impurity enhances the binding energy of the nickel cluster, reduces their magnetic moment, and decreases the ionization potential. We find that the geometries of the host clusters do not change significantly after the addition of the tin atom, except for the case of Ni_6. The tin impurity prefers to sit on sites which can maximize the number of Sn–Ni bonds, and occupies vertex sites.

I. INTRODUCTION

In recent years, the field of atomic clusters has received widespread attention.[1–3] Their properties are known to evolve nonmonotonically with size. An understanding of the evolution of the equilibrium geometries and its relationship to the underlying electronic structure are, therefore, of central importance. Many of these properties can be changed by doping the clusters or mixing the clusters with other species. The rich diversity of mixed alloys, especially in extended systems, has lead to their widespread application in electronics and electrocatalytic processes. In this context, bimetallic clusters containing transition metal atoms are of special interest due to their potential role in catalysis and magnetism.

The nickel-tin system forms an important class of intermetallic compounds with high oxidation and corrosion resistance. Huber *et al.*[4] discovered a heterogeneous catalyst based on Ni, Sn, and Al, which is useful for various hydrocarbon reactions. A significant amount of experimental and theoretical studies on the deposition of tin on the nickel surfaces has been conducted due to its importance in electronics and catalytic processes.[5–13] It is found that Sn-Ni(1 1 0)c (2×2) surface alloy is energetically the most favorable, where Sn atoms substitute Ni atoms in the outermost layers.[13] The binary clusters consisting of nickel and tin atoms are expected to provide useful prototype models to understand the physics and chemistry of surfaces and nanostructures. The smaller size of the clusters makes it possible to obtain a detailed information about the geometry, electronic structure, and the nature of bonding. However, there is a dearth of both theoretical and experimental works on nickel-tin at the cluster level. A few theoretical studies have been reported on small Ni_nSn clusters, $n \leq 6$.[14–16] For example, the structural and vibrational properties on neutral Ni_nSn $(n \leq 4)$ have been reported earlier using density functional formalism.[14] Our aim is to perform a systematic study of the evolution of the structural, electronic, and magnetic properties of Ni clusters containing a single tin impurity. In this work, we present the results of density functional calculations on neutral and ionized clusters of Ni_nSn in the size range of $n=1-12$. In the following section (Sec. II), we describe in brief the computational details, which is followed

by the discussion of our results in Sec. III. In Sec. IV, conclusions are presented.

II. COMPUTATIONAL DETAILS

All the calculations have been performed using spin density functional theory within the pseudopotential plane wave method. We have used projector augmented wave (PAW) method[17,18] and two different exchange-correlation functionals: the local spin density approximation of Vosko, Wilk, and Nusair[19] (VWN) and generalized gradient approximation (GGA) given by Perdew and Wang (PW-91)[20] as implemented in the VASP package.[21] The clusters were placed in a cubic supercell with an edge of 20 Å, and periodic boundary conditions were imposed. The cutoff energy for the plane wave was set to 269.56 eV. The optimized geometries of the clusters were obtained by quenching the various planar and three-dimensional (3D) configurations using the quasi-Newton-Raphson method.[21] At least 20 initial configurations were considered for larger clusters. The structures were considered to be converged when the force on each ion was less than 0.01 eV/Å, with a convergence in the total energy of about $10^{-4}-10^{-6}$ eV. In all the cases, the lowest-energy structure has been confirmed by changing the positions of Ni and Sn atoms, as well as by considering the configurations of the Ni clusters available from the previous studies.[22–29] The equilibrium geometries of the stable neutral clusters are considered as a starting point for the geometry optimization of the ionized aggregates. The stability of the lowest-energy configuration and the isomers of a given cluster is further checked by performing calculations with different spin states.

III. RESULTS

In this section, we present the equilibrium structures, the stability, energetics, and the magnetic moments of the Ni_nSn neutral and ionic clusters $(n=1-12)$. The equilibrium structures of Ni_nSn clusters along with Ni_{n+1} geometries $(n=2-12)$ are shown in Figs. 1 and 2. Before beginning our discussion, we note that the ionic radii of the Ni and Sn atoms are 0.69 and 0.71 Å, respectively. The binding
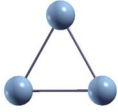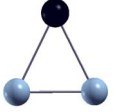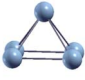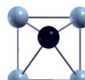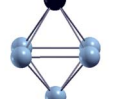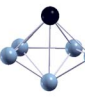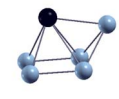
FIG. 1. (Color online) The ground-state geometries of Ni_{n+1} clusters (column 2). The structures on the right side show the lowest-energy structure (column 3) and some of the low-lying configurations for Ni_nSn clusters ($n=2-7$). n (column 1) represents the total number of Ni atoms in Ni_nSn clusters. The lightly shaded spheres represent the Ni atoms, and the dark sphere represents the Sn atom. The energies are in eV and the magnetic moments are in μ_B.

energy (BE) of NiSn dimer (1.85 eV/atom) is larger than Ni_2 (1.46 eV/atom). The dimer bond lengths of Ni-Sn and Ni-Ni are 2.27 and 2.09 Å, respectively. The anionic NiSn is found to be more (BE=2.90 eV/atom) stable than the neutral NiSn with R_{Ni-Sn} distance of 2.33 Å. This is consistent with the picture given by the molecular orbitals. The electron added to the neutral NiSn occupies the lowest unoccupied molecular orbital (LUMO), which has a bonding character. For the cationic case, the ionized electron comes out from a deeper bonding orbital of the neutral NiSn. It therefore results in the less stable configuration.

The lowest-energy configuration of Ni_2Sn is found to be an isosceles triangle, similar to that of Ni_3. The other two linear configurations Sn-center (Ni-Sn-Ni) and Ni-center (Ni-Ni-Sn) are well above the triangular configuration ($\Delta E=1.0$ and 1.69 eV, respectively). The triangular configuration

maximizes the overall number of bonds (both Ni-Ni and Ni-Sn) as compared to the other linear isomers. By preferring 3D configuration, Ni_3Sn follows the same trend as that of Ni_2Sn. The overall number of bonds increases in 3D configuration as compared to a planar rhombus configuration. The planar rhombus structure is 0.32 eV higher in energy than the pyramid configuration. To focus on the stability of 3D configuration, we have examined the isodensity surfaces of the molecular orbitals of 3D and rhombus structures. In our discussion, a typical occupied orbital is denoted by the notation HOMO-n, where n represents the number of level counted from highest occupied molecular orbital (HOMO). Figure 3 shows the isodensity surface for HOMO-17 of the pyramidal structure. In the case of the 3D configuration, a strong localization region is identified at the center of three Ni atoms, indicating a three-centered bonding region. This
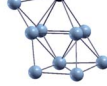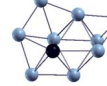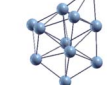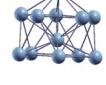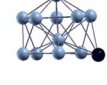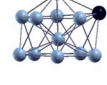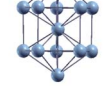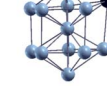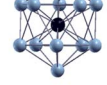
| n | Ni_{n+1} | Ni_nSn | $(n = 8 - 12)$ | |

FIG. 2. (Color online) Ground-state geometries of Ni_{n+1} clusters (column 2). The structures on the right side show the lowest-energy structure (column 3) and some of the low-lying configurations for Ni_nSn clusters ($n=8$–12). n (column 1) represents the total number of Ni atoms in Ni_nSn clusters. The lightly shaded spheres represent the Ni atoms, and the dark sphere represents the Sn atom. The energies are in eV and the magnetic moments are in μ_B.

makes the 3D configuration more stable as compared to the planar one.

The lowest-energy structure of Ni_4Sn is a triangular pyramid configuration. The square pyramid configuration is nearly degenerate with the lowest-energy configuration ($\Delta E = 0.01$ eV). For Ni_5Sn, the ground-state structure is a slightly distorted octahedron configuration, where a Sn atom is at the vertex position. The capped trigonal pyramid and capped tetrahedron configurations of Ni_5Sn are the other low-lying structures at higher energies by 0.02 and 0.13 eV, respectively. Ni_6Sn is a pentagonal bipyramid, while Ni_7 has a capped octahedron structure. Our calculations found that for Ni_7, the capped octahedron is 0.16 eV lower in energy than the pentagonal bipyramid structure. This is consistent with the previous theoretical[30,31] and experimental[28] results. A capped octahedron configuration of Ni_6Sn is 0.2 eV higher in

energy than the pentagonal bipyramid structure. The lowest-energy structure of Ni_7Sn is found to be a bicapped octahedron configuration. This trend of capping continues with the addition of Ni atom up to $n=12$. The tendency for the formation of a pentagonal ring is seen from $n \geqslant 6$.

For $Ni_{12}Sn$, the lowest-energy structure is the icosahedral configuration, where the Sn atom is at vertex position. The next low-lying configuration is 0.7 eV higher in energy with D_{5h} symmetry. Even though for the lowest (I_h) and next low-lying (D_{5h}) configurations, the coordination number of Sn is the same, the R_{Sn-Ni} distance from vertex Sn to center Ni atom increases from 2.65 to 2.83 Å, and the overall Ni-Ni distance increases by 3% as compared to the icosahedron structure. This increase in Ni-Sn and Ni-Ni bond lengths makes the cluster relatively unstable. The icosahedral configuration with the Sn atom at the center site is well above
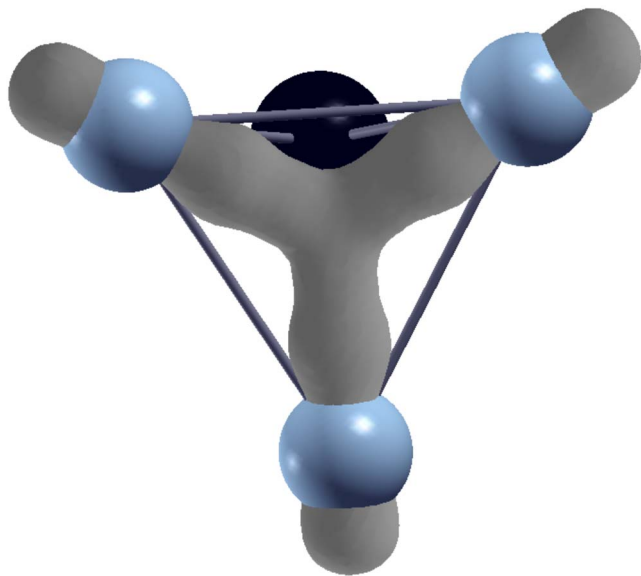
FIG. 3. (Color online) Isodensity surface corresponding to the HOMO-17 state for the lowest-energy configuration of Ni_3Sn, at one-third of its maximum isosurface value.

FIG. 4. Binding energy per atom (eV) for neutral, ionic Ni_nSn ($n=1-12$), and Ni_{n+1} clusters vs number of atoms in the cluster.

the lowest-energy structure (3.6 eV). It is found that if a larger Sn atom is placed at the center of the icosahedron, the cluster would undergo a slight expansion; this would reduce the Ni-Sn and Ni-Ni interactions. The minimum R_{Ni-Sn} distance increases by 5% as compared to the lowest-energy configuration. Thus, the atomic size mismatch appears to be the origin of the higher stability of the $Ni_{12}Sn$ configuration, where Sn is at the vertex position. This observation is consistent with previous studies[32,33] on nickel clusters with boron and aluminum impurities. The larger size Al atom prefers the vertex site in the nickel cluster, while the smaller boron atom prefers to go at the center of the nickel cluster.

The overall evolutionary trend for the Ni_nSn series shows that, except for $n=6$, the Sn doped geometries are similar to those of Ni_{n+1} clusters, where the Sn atom occupies a substitutional surface site accompanied with a slight distortion in the host cluster. It is seen that Sn prefers to maximize the Ni-Sn bonds by selecting that site which increases the coordination of Ni with Sn. It is also seen that from $n \geqslant 7$, the cluster minimizes energy by maximizing Ni-Ni bonds. Our results for Ni_nSn geometries are similar to the earlier reported[14–16] geometries, except for $n=6$. This difference is clearly due to the strategy used in their work. They have performed a symmetry constrained optimization.

All the ground-state configurations of anionic and cationic Ni_nSn clusters ($n \leqslant 12$) (not shown) are similar to those of neutral configurations, except for Ni_4Sn^- and Ni_7Sn^+. The anionic Ni_4Sn tetrahedral configuration is more stable as compared to the triangular configuration ($\Delta E=0.01$ eV). The distorted capped pentagonal bipyramidal configuration of Ni_7Sn^+ is more stable than the Archimedian antiprism (T_d) ($\Delta E=0.21$ eV). These structural change can be explained on the basis of the electronic structure of the cluster, which will be discussed in the next section. It is also found that, when the cation is formed, the Ni-Sn bond lengths increase with
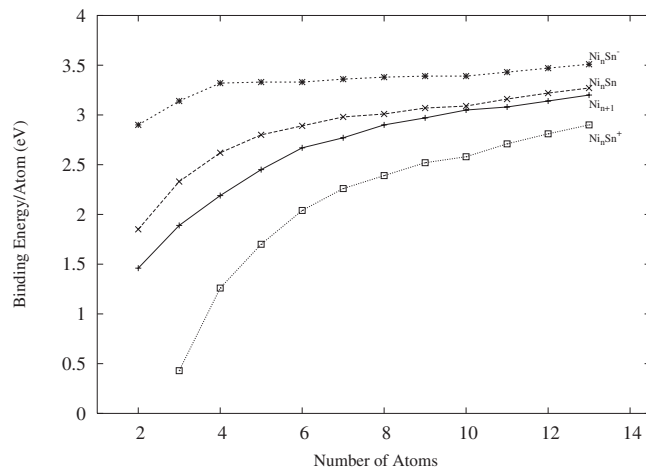
respect to the neutral cluster, while the addition of electron enhances the Ni-Sn interactions by decreasing the Ni-Sn bond lengths. The stability of neutral and ionic clusters can be found by examining the binding energy per atom (E_b).

The BE is calculated as

$$E_b[Ni_nSn] = (-E[Ni_nSn] + nE[Ni] + E[Sn])/(n+1), \quad (1)$$

where E is the total energy of the system.

The binding energy per atom (in eV) for Ni_nSn neutral and ionic clusters against the number of atoms is shown in Fig. 4. For comparison, we have also plotted the binding energy per atom (in eV) for Ni_{n+1} cluster, which clearly indicates that the substitution of the Ni atom by Sn enhances the binding energy of the given cluster. Up to $n=6$, for Sn doped clusters, the BE increases substantially as compared to the binding energy of the host cluster. After $n>6$, it increases with n, but finally tends to saturate. This indicates that the structures are stabilized with the coordination of six Ni atoms for the Sn, for clusters with $n>6$. The BE curves for anionic and cationic clusters show a similar nature as that of the neutral clusters. As noted earlier, an addition of one electron increases the Ni-Sn interaction by decreasing the Ni-Sn bond lengths in anionic clusters. This will enhance the binding energy of $(Ni_nSn)^-$ as compared to a neutral one as well as compared to the host clusters. However, the removal of electron decreases the Ni-Sn interaction, which results in less stability for the cationic clusters.

The stability of these clusters is also analyzed by examining fragmentation energies. Here, we consider two fragmentation channels involving either a Ni atom or a Sn atom. The fragmentation energies for a neutral Ni_nSn cluster are calculated as

$$\Delta^1 E[Ni_nSn] = E[Ni_nSn] - (E[Ni_n] + E[Sn]), \quad (2)$$

$$\Delta^2 E[Ni_nSn] = E[Ni_nSn] - (E[Ni_{n-1}Sn] + E[Ni]), \quad (3)$$

where E is the total energy of the system.

Figure 5 shows the fragmentation energies for the Ni_nSn cluster with respect to Ni and Sn atoms. Δ^1 is the energy gain
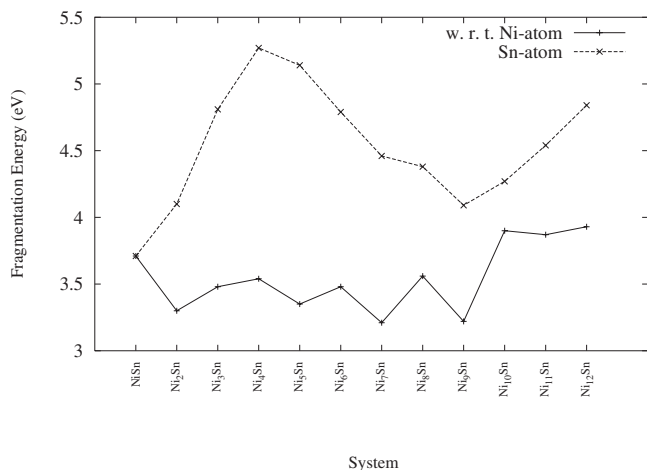
FIG. 5. Fragmentation energies (eV) of Ni_nSn clusters ($n = 1-12$) via loss of a Ni atom and a Sn atom.

in adding a Sn atom to a Ni_n cluster, and Δ^2 the energy gain in adding a Ni atom to a $Ni_{n-1}Sn$ cluster. It is found that for Sn induced clusters, the energetically lowest fragmentation channel corresponds to the loss of a single Ni atom. Δ^2 gives the number of how many Ni atoms can be bonded to a single Sn atom. It is 3.54 eV for Ni_4Sn, and the lowest 3.22 eV for Ni_9Sn. These behaviors of Δ^1 and Δ^2, and more precisely, $\Delta^1 \gg \Delta^2$ for all n, indicate that the addition of Sn to a Ni cluster is energetically favorable.

The total magnetic moment for Ni_nSn clusters against the number of atoms in the cluster is shown in Fig. 6, where we have also plotted the total moment of the host nickel clusters. It is seen that the doping of the Sn atom reduces the magnetic moment of the nickel clusters. The overall magnetic moment of the Ni_nSn series varies considerably with the number of atoms in the cluster. For the NiSn dimer, it is 0; it increases up to $7\mu_B$ for $n = 12$. It is found that the spin state of the Ni_nSn cluster appears to depend on the placement of the tin atom, the Ni-Ni interactions, and the nature of the
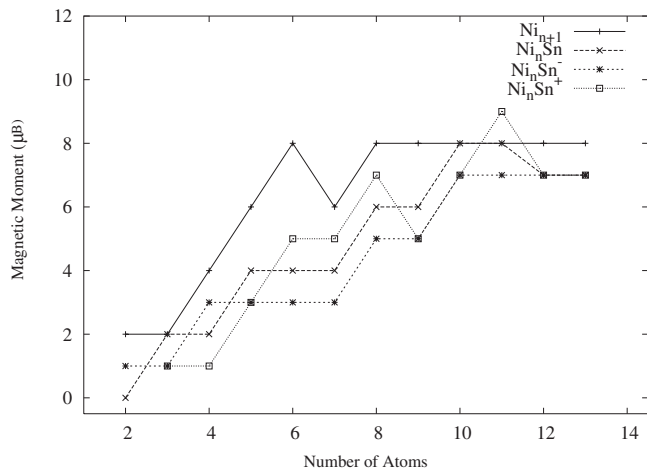

FIG. 6. Total magnetic moment (in μ_B) for the neutral, ionic Ni_nSn ($n = 1-12$), and Ni_{n+1} structures as a function of number of atoms in the cluster.
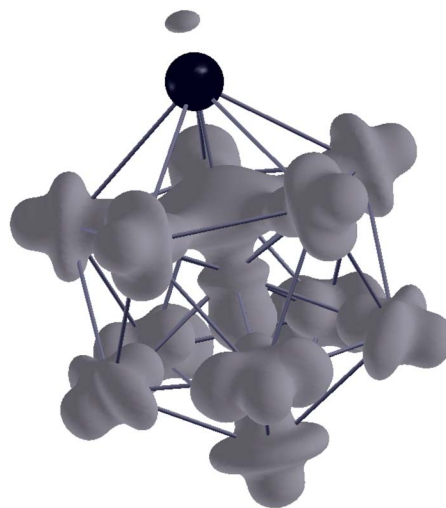

FIG. 7. (Color online) Isodensity surface corresponding to the HOMO-55 state of $Ni_{12}Sn$ lowest-energy configuration, where a Sn atom is at the vertex site.

hybridization of Sn p with Ni d complex. For example, the magnetic moment of the lowest-energy configuration of Ni_4Sn is $4\mu_B$, while for the planar isomer it is $2\mu_B$. In the case of Ni_7Sn, the lowest-energy configuration, the total magnetic moment is $6\mu_B$, while for the nearly degenerate next low-lying configuration (0.03 eV), it reduces to $4\mu_B$. These variations are further illustrated by considering different configurations of the $Ni_{12}Sn$ cluster, where the placement of the Sn atom, the cluster symmetry, significantly changes the magnetic moment of the cluster.

As noted earlier, the Sn-vertex icosahedra is 0.7 eV lower in energy as compared to the Sn-vertex $Ni_{12}Sn$ configuration with D_{5h} symmetry. The magnetic moment of lowest-energy icosahedral configuration is $7\mu_B$, while for the next low-lying configuration, it is $9\mu_B$, which is higher than the magnetic moment of Ni_{13} cluster ($8\mu_B$). The Sn-center icosahedra is at a higher energy (3.6 eV) as compared to the Sn-vertex icosahedral configuration. For Sn-center icosahedral structure, the coordination number of the Sn atom is 12. This increase in coordination as compared to the lowest-energy configuration decreases the magnetic moment to $4\mu_B$. All these remarks are further explained by considering the nature of bonding in these clusters.

We have examined the charge density isosurfaces of the molecular orbitals, the eigenvalue spectrum (not shown) for the lowest-energy configuration, and some of the low-lying configurations of all clusters. The localized charge density distribution is found around Ni atoms. This is consistent with the fact that Ni (1.12) has a greater electron affinity than Sn (1.07). The charge transfer is observed from Sn to Ni atoms. The HOMO of all the lowest-energy configurations belongs to Ni d, and the tin atom induces the density of states at the middle of the energy spectrum due to hybridization of Sn p with Ni d. A typical state from the lowest-energy configuration of $Ni_{12}B$ is shown in Fig 7. It is seen that the Sn p hybridizes with six Ni d_{z^2}.

As mentioned earlier, the icosahedron configuration is 0.7 eV lower in energy as compared to the cluster with D_{5h}
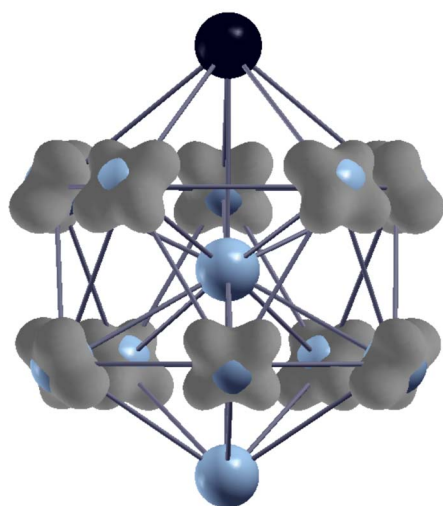
(a)
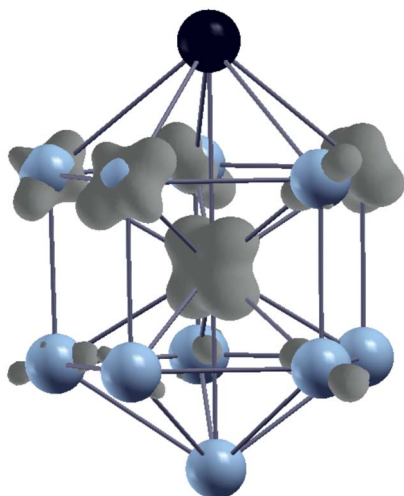
(b)

FIG. 8. (Color online) HOMO isodensity surface (a) for lowest-energy configuration ($Ni_{12}Sn$-I_h) and (b) for next low-lying configuration ($Ni_{12}Sn$-D_{5h}).

symmetry. Figures 8(a) and 8(b) show the isodensity for the HOMOs of two isomers of $Ni_{12}Sn$ with different symmetries. It is seen that for the lowest-energy configuration, the HOMO is dominated by $d_{x^2-y^2}$, and the Sn, central Ni, and vertex Ni atoms are not participating in the hybridization. For the next low-lying configuration, the mixture of $d_{x^2-y^2}$ and d_{z^2} is observed on the nickel atoms, and here, the central Ni atom is also participating in the hybridization. The mixture of d orbitals and the inhomogeneous distribution of charge density lead to an increase in magnetic moment,
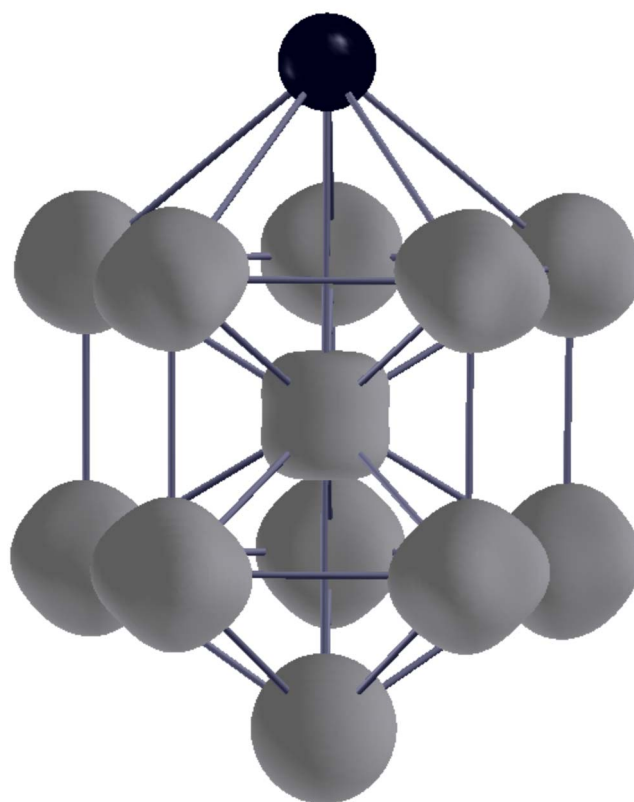

FIG. 9. (Color online) The spin density $[\rho_\uparrow(\mathbf{r})\text{-}\rho_\downarrow(\mathbf{r})]$ isosurface of the low-lying configuration of $Ni_{12}Sn$ (D_{5h}), at one-sixth of its maximum isosurface value.

which has already been discussed. Figure 9 shows the spin density $[\rho_\uparrow(\mathbf{r})-\rho_\downarrow(\mathbf{r})]$ for this low-lying configuration. The magnetization density is seen on all Ni atoms including the central one. It is already noted that for $Ni_{12}Sn$-D_{5h}, there is a 6% increase in Ni-Sn distance from vertex Sn to central Ni atom as compared to $Ni_{12}Sn$-I_h configuration. This decrease in Ni-Sn interaction induces the magnetization on the central Ni atom.

The analysis of the molecular orbitals for anionic and cationic clusters shows similar findings as those of the dimer. When the electron is added to the neutral Ni_nSn cluster, it occupies the LUMO, which has a bonding character. This leads to an enhancement in stability and a decrease in the magnetic moment of anionic clusters. On the other hand, the electron comes out from the deeper bonding orbital of the neutral Ni_nSn cluster, which makes the cationic cluster less stable as compared to the neutral one.

We have also calculated the adiabatic electron affinity (EA) and the ionization potential (IP). Adiabatic electron affinity (AEA) is defined as the energy difference between the anionic and neutral clusters in their respective optimized geometries, while the adiabatic ionization potential (AIP) is defined as the energy difference between the cationic and neutral clusters in their respective optimized geometries. Vertical electron affinity (VEA) is defined as the energy difference between the anionic and neutral clusters with both at the optimized geometry of the anionic cluster, while the vertical ionization potential (VIP) is defined as the energy dif-

TABLE I. Adiabatic and vertical values (eV) of the ionization potential and electron affinity for Ni_nSn clusters ($n=1-12$) along with the vertical ionization potential of Ni_{n+1} cluster (Ref. 25).

System	n											
	1	2	3	4	5	6	7	8	9	10	11	12
VIP-Ni_{n+1}	8.3	6.8	5.9	6.6	6.8	6.4	6.5	6.5	6.2	6.1	6.1	6.3
AIP		5.74	5.45	5.51	5.16	5.08	4.97	4.93	5.11	4.99	4.86	4.83
VIP		5.7	5.46	5.55	5.18	5.09	5.20	4.95	5.11	5.01	4.87	4.83
AEA	2.08	2.40	2.80	2.60	2.58	2.63	2.94	2.87	3.08	3.07	3.08	3.10
VEA	2.10	2.42	2.80	2.62	2.59	2.64	2.95	2.87	3.08	3.00	3.09	3.10

ference between the cationic and neutral clusters with both at the optimized geometry of the neutral cluster.

Table I shows the calculated IP and the EA of the Ni_nSn clusters. The IPs show a decrease from NiSn to $Ni_{12}Sn$, while EAs increase with n. The vertical and adiabatic EAs and IPs are nearly the same, which indicates that there is not much structural differences between neutral and ionic configurations of Ni_nSn clusters. Our calculated values of IPs and EAs agree qualitatively with the reported calculations by Finetti et al.[15,16] Reddy et al.[25] computed the vertical ionization potential of Ni_n clusters using a self-consistent molecular orbital theory. For comparison, we have also noted their results for the vertical ionization potential of nickel clusters. It clearly indicates that doping with Sn atom reduces the ionization potential of nickel clusters.

It would be interesting to further investigate the effect on geometries and on the electronic properties of nickel clusters of more number of Sn atoms. The work involving mixed Ni-Sn clusters is being performed to investigate more deeply the effect of Sn on nickel clusters.

IV. CONCLUSIONS

In the present investigation, we have reported the lowest-energy configuration and some of the low-lying configurations of Ni_nSn ($n=1-12$) using spin density functional theory. The overall evolutionary trend shows that, except $n=6$, the geometries of doped clusters are similar to those of Ni_{n+1}, where the Sn atom occupies the vertex site, accompanied by a slight distortion in the cluster. The doping by tin atom increases the binding energy and reduces the magnetic moment and the ionization potential of the nickel cluster. The structural stability and magnetic properties of these clusters appear to be the outcome of a delicate interplay among the coordination number of the Sn atom, the cluster symmetry, and the hybridization of Sn p and Ni d orbitals.

*Corresponding author; d_mrinal@yahoo.com

[1] V. Kumar, K. Esfarjani, and Y. Kawazoe, *Clusters and Nanomaterials*, Springer Series in Cluster Physics (Springer-Verlag, Berlin, Heidelberg, 2002).

[2] *Clusters and Nanostructured Materials*, edited by P. Jena and S. N. Behera (Nova Science, New York, 1996).

[3] J. A. Alonso, Chem. Rev. (Washington, D.C.) **100**, 637 (2000).

[4] G. W. Huber, J. W. Shabaker, and J. A. Dumesic, Science **300**, 2075 (2003).

[5] A. Onda, T. Komatsu, and T. Yashima, Phys. Chem. Chem. Phys. **2**, 2999 (2000).

[6] Tuan-Chi Liu and Shwu-Jer Chiu, Ind. Eng. Chem. Res. **33**, 488 (1994).

[7] M. L. Ferreira, N. N. Nichio, and O. A. Ferretti, J. Mol. Catal. A: Chem. **202**, 197 (2003).

[8] J. W. Shabaker, D. A. Simonetti, R. D. Cortright, and J. A. Dumesic, J. Catal. **231**, 67 (2005).

[9] S. H. Overbury and Yi-sha Ku, Phys. Rev. B **46**, 7868 (1992).

[10] Y. D. Li, L. Q. Jiang, and B. E. Koel, Phys. Rev. B **49**, 2813 (1994).

[11] M. Masai, K. Mori, H. Muramoto, T. Fujiwara, and S. Ohnaka, J. Catal. **50**, 419 (1977).

[12] C. Schmetterer, H. Flandorfer, K. W. Richter, U. Saeed, M. Kauffman, P. Roussel, and H. Ipser, Intermetallics **15**, 869 (2007).

[13] D. F. Li, H. Y. Xiao, X. T. Zu, and H. N. Dong, Mater. Sci. Eng., A **460**, 50 (2007).

[14] M. Finetti, E. E. Ottavianelli, R. Pis Diez, and A. H. Jubert, Comput. Mater. Sci. **20**, 57 (2001).

[15] M. Finetti, E. E. Ottavianelli, R. Pis Diez, and A. H. Jubert, Comput. Mater. Sci. **25**, 363 (2002).

[16] M. Finetti, E. E. Ottavianelli, R. Pis Diez, and A. H. Jubert, THEOCHEM **634**, 171 (2003).

[17] P. E. Blochl, Phys. Rev. B **50**, 17953 (1994).

[18] G. Kresse and D. Joubert, Phys. Rev. B **59**, 1758 (1999).

[19] S. H. Vosko, K. Wilk, and N. Nusair, Can. J. Phys. **58**, 1200

(1980).

[20] J. P. Perdew and Y. Wang, J. Chem. Phys. **45**, 13244 (1992).

[21] Vienna *ab initio* Simulation Package (VASP) (Technische Universität Wien, 1999).

[22] F. A. Reuse and S. N. Khanna, Chem. Phys. Lett. **234**, 77 (1995).

[23] F. A. Reuse, S. N. Khanna, and S. Bernel, Phys. Rev. B **52**, R11650 (1995).

[24] S. K. Nayak, S. N. Khanna, B. K. Rao, and P. Jena, J. Phys. Chem. A **101**, 1072 (1997).

[25] B. V. Reddy, S. K. Nayak, S. N. Khanna, B. K. Rao, and P. Jena, J. Phys. Chem. A **102**, 1748 (1998).

[26] S. N. Khanna, M. Beltran, and P. Jena, Phys. Rev. B **64**, 235419 (2001).

[27] M. Moskovits and J. E. Hulse, J. Chem. Phys. **66**, 3988 (1977).

[28] E. K. Parks, L. Zhu, J. Ho, and S. J. Riley, J. Chem. Phys. **100**, 7206 (1994); **102**, 7377 (1995).

[29] L. Lian, C.-X. Su, and P. B. Armentrout, J. Chem. Phys. **96**, 7542 (1992).

[30] S. K. Nayak, B. Reddy, B. K. Rao, S. N. Khanna, and P. Jena, Chem. Phys. Lett. **253**, 390 (1996).

[31] E. Curotto, A. Matro, and D. L. Freeman, J. Chem. Phys. **108**, 729 (1998).

[32] E. F. Rexer, J. Jellinek, E. B. Krissinel, E. K. Parks, and S. J. Riley, J. Chem. Phys. **117**, 82 (2002).

[33] M. Deshpande, D. G. Kanhere, and Ravindra Pandey, Phys. Rev. A **71**, 063202 (2005).